Electronic Supplementary Information

Co-synthesis of atomically precise nickel nanoclusters and the pseudo optical gap of $Ni_4(SR)_8$

Yanze Pan‡, Jishi Chen‡, Shida Gong, Zonghua Wang*

Shandong Sino-Japanese Center for Collaborative Research of Carbon Nanomaterials, College of Chemical Science and Technology, Qingdao University, Qingdao 266071, China

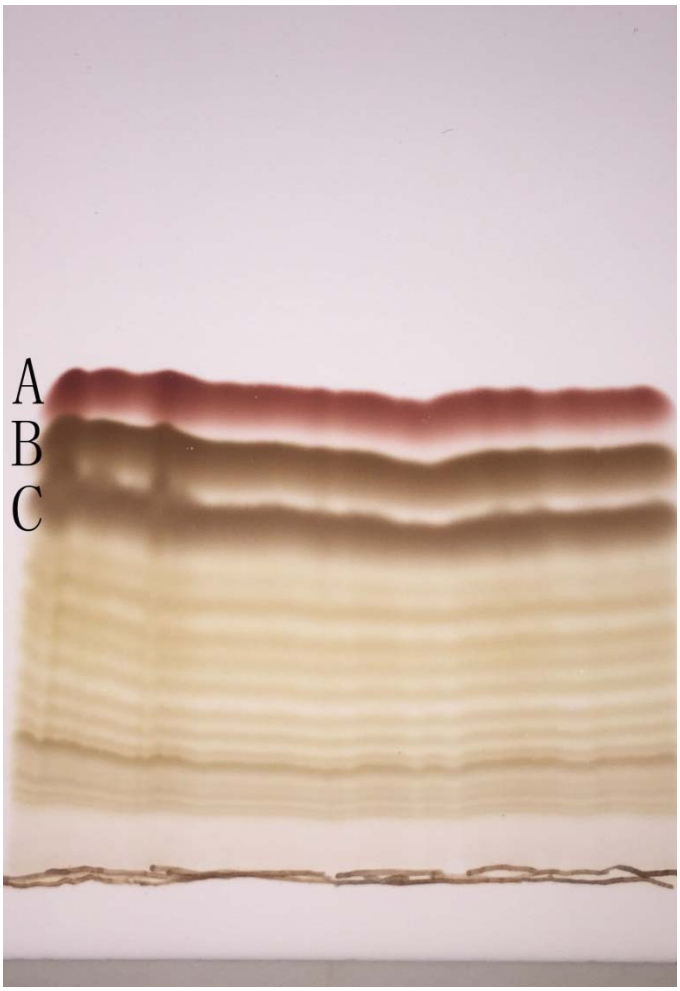

Fig. S1 PTLC of product A, B and C synthesized by one-pot method with *n*-propanol as solvent.

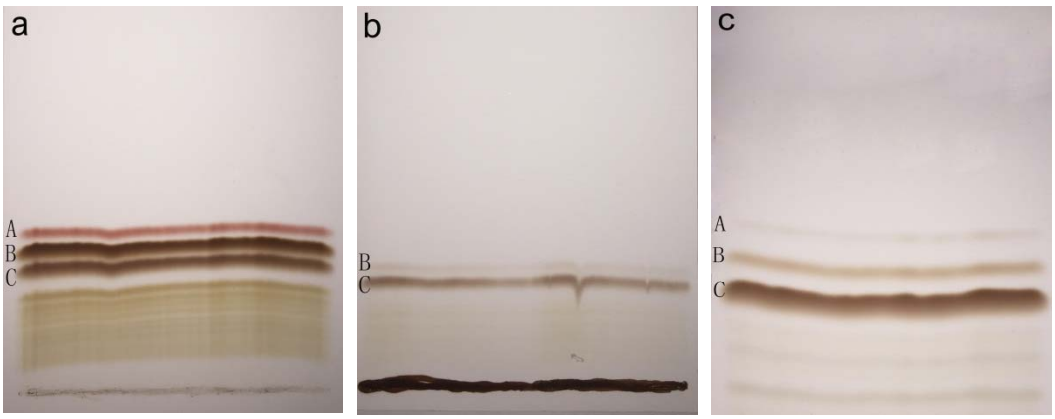

Fig. S2 PTLC of product A, B and C synthesized by one-pot method with THF (a) and acetonitrile (b) as solvent, and by the modified Brust-Schiffrin method with THF as solvent (c). Comparing the main product synthesized by one-pot method with different solvent, when using THF as solvent, three products were obtained and the relative yield of product A is less than that with *n*-propanol as solvent; but when with acetonitrile as solvent, most of reaction product are not dissolve in CH_2Cl_2 and the soluble product only contains product C and product B. Comparing with the reaction products synthesized by one-pot method and the modified Brust-Schiffrin method with THF as solvent, we find that product A, B and C were appearing in both of their products, but the relative yields of product B and A synthesized by modified Brust-Schiffrin method are less than that by one-pot method.

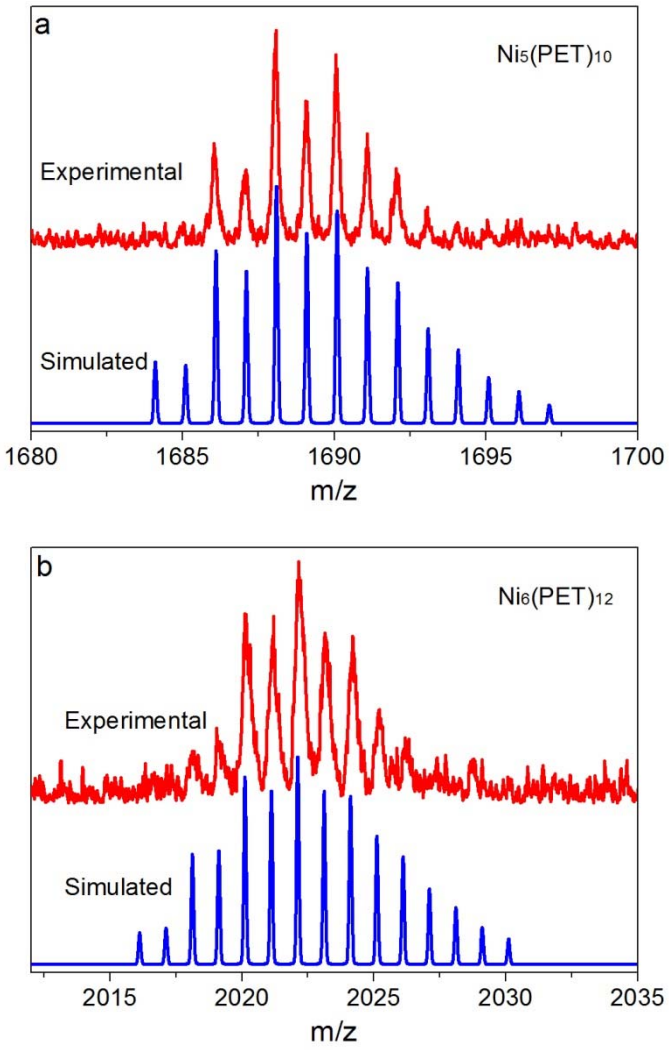

Fig. S3 The comparison of simulated and experimentally obtained isotopic patterns of $Ni_5(PET)_{10}$ (a) and $Ni_6(PET)_{12}$ (b). As shown in these figures, the deviation between two adjacent peaks is 1 Da, indicating these adducts own one positive charge.

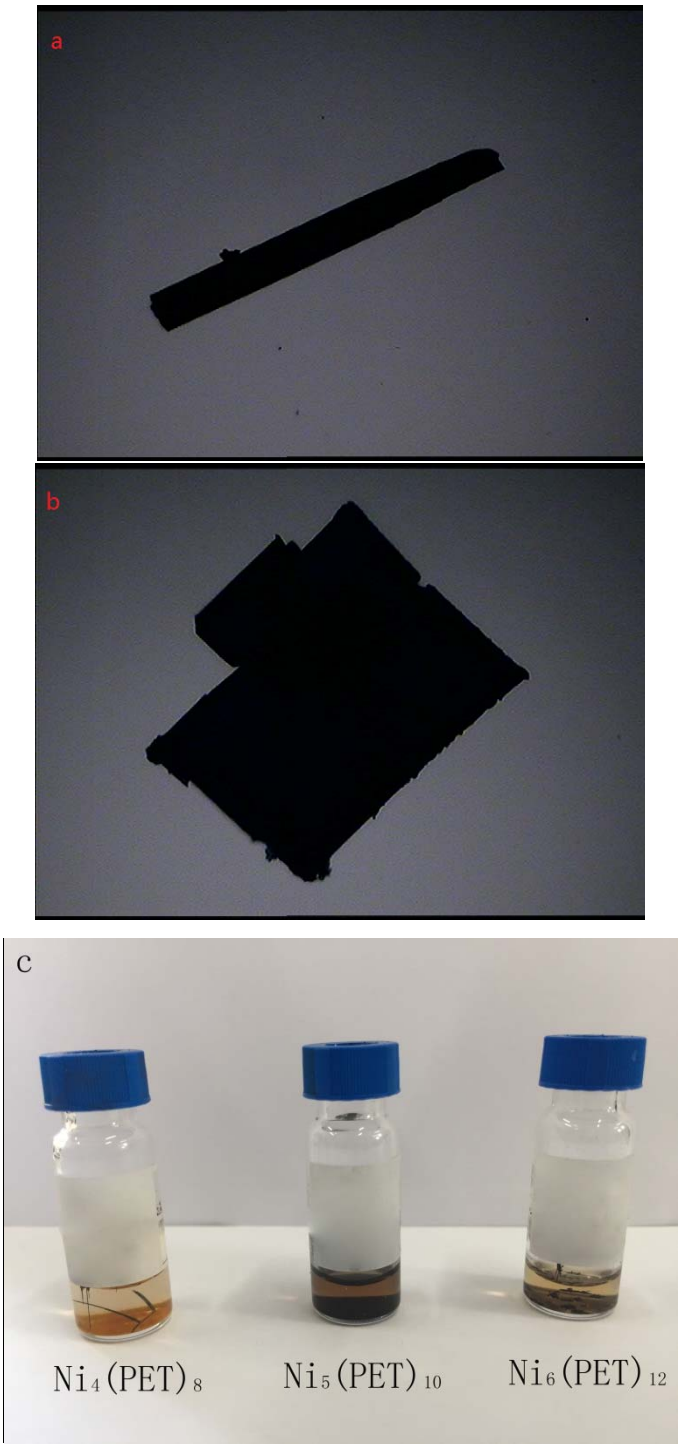

Fig. S4 The photographs of needle-shaped $Ni_4(PET)_8$ crystal (a) and flake-shaped $Ni_6(PET)_{12}$ crystal, and the solutions of $Ni_4(PET)_8$, $Ni_5(PET)_{10}$ and $Ni_6(PET)_{12}$ after crystal growth (c). We can find in Fig. S4c that after crystallized for one week under the same condition, only needle-shaped crystal appeared in the solution of $Ni_4(PET)_8$ and flake-shaped crystal in the solution of $Ni_6(PET)_{12}$, but no crystal appeared in the solution of $Ni_5(PET)_{10}$.

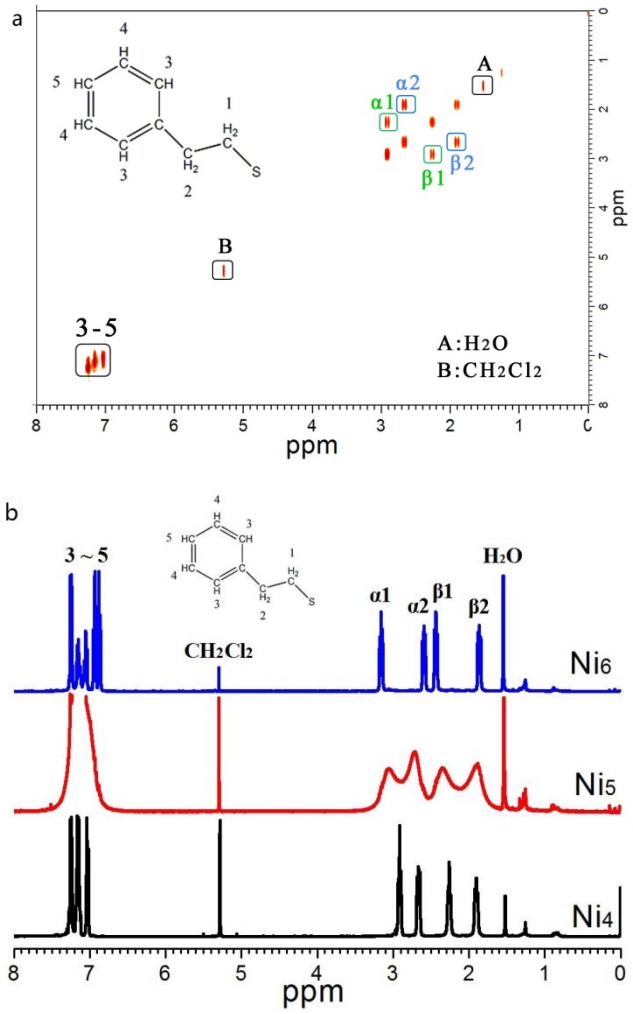

Figure S5. 2D COSY of $Ni_4(PET)_8$ (a) and ^1H NMR spectra of $Ni_4(PET)_8$, $Ni_5(PET)_{10}$ and $Ni_6(PET)_{12}$ (b).

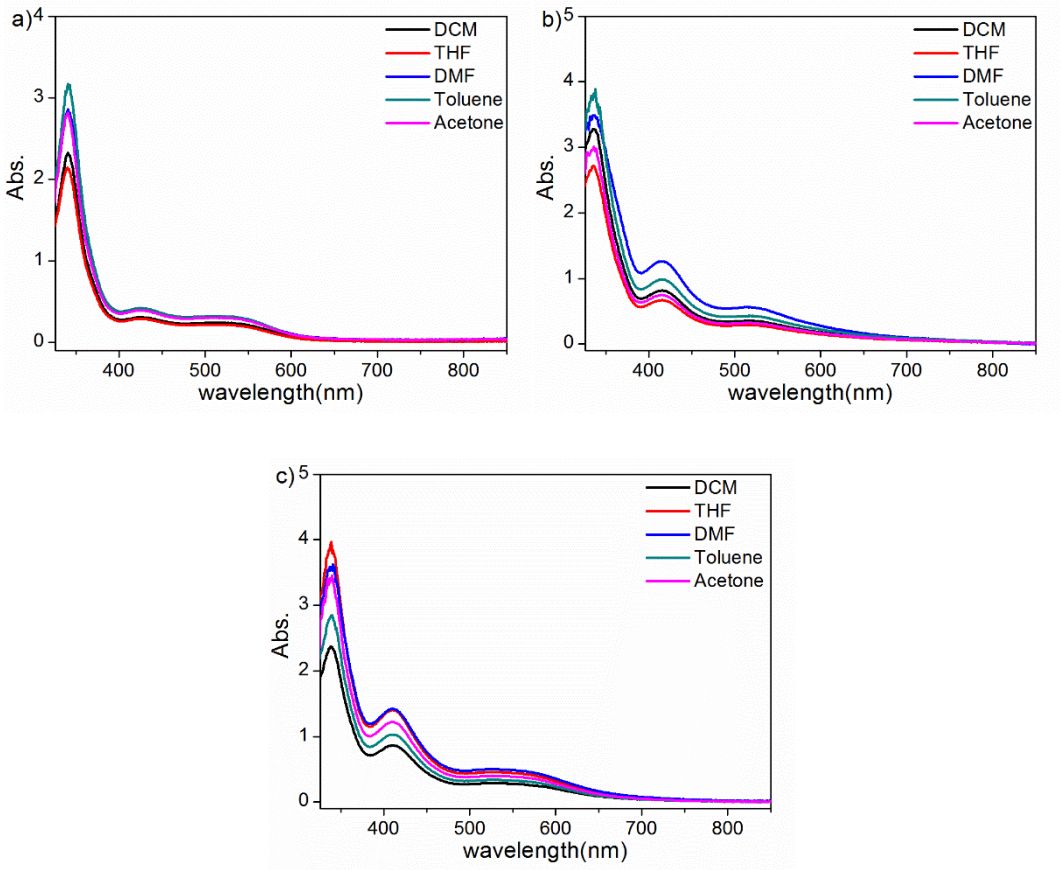

Figure S6. The UV/Vis/NIR absorption spectra of $Ni_4(PET)_8$ (a), $Ni_5(PET)_{10}$ (b) and $Ni_6(PET)_{12}$ (c) dissolved in different solvent. DCM: CH_2Cl_2, THF: tetrahydrofuran, DMF: N,N-Dimethylformamide.

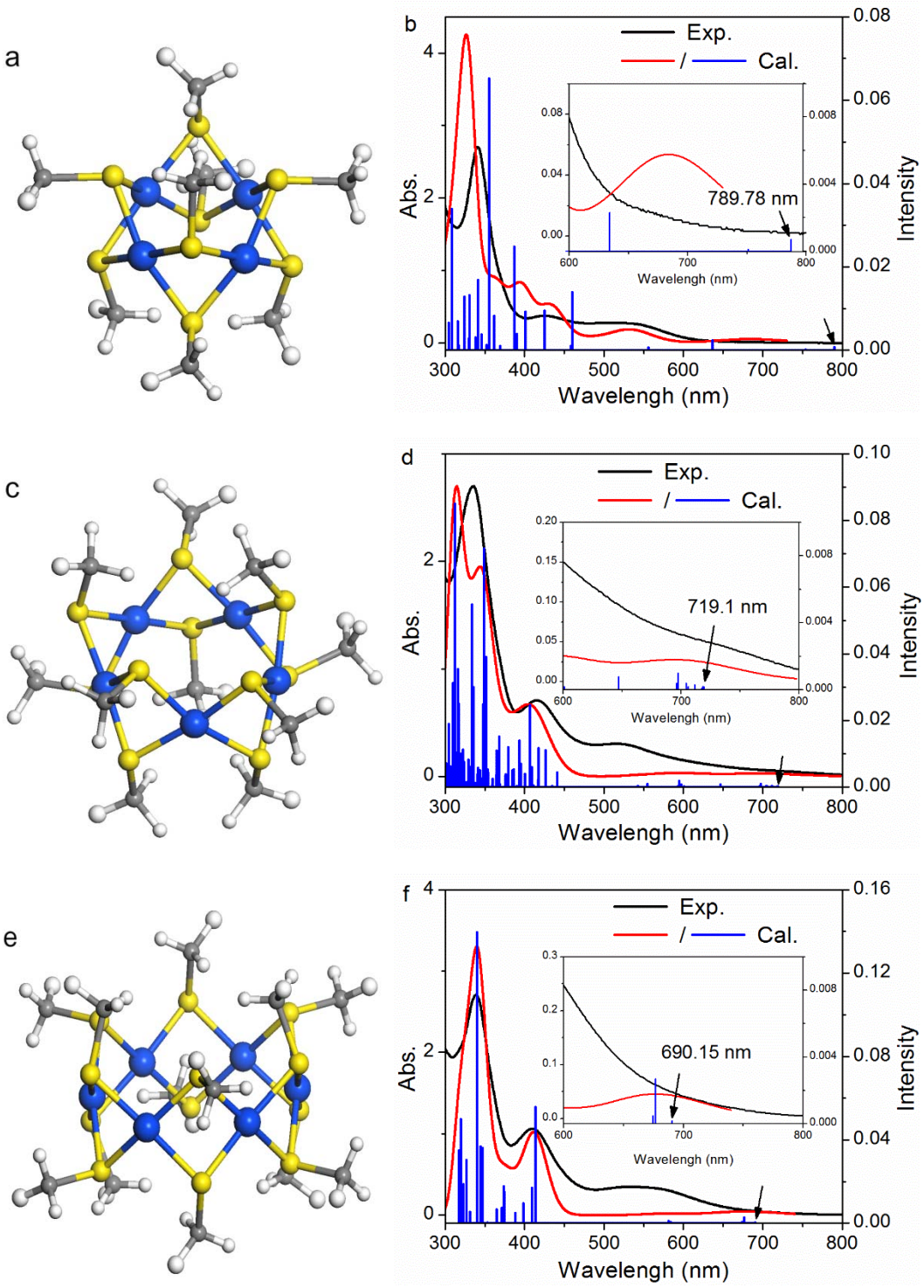

Figure S7. The optimized structures of $Ni_4(SCH_3)_8$ (a), $Ni_5(SCH_3)_{10}$ (c) and $Ni_6(SCH_3)_{12}$ (e) nanoclusters by DFT calculation and the UV/Vis/NIR spectra of theoretical calculations and experimental test of $Ni_4(PET)_8$ (b), $Ni_5(PET)_{10}$ (d) and $Ni_6(PET)_{12}$ (f). Inset of (b), (d) and (f), the UV/Vis/NIR spectra in the range from 600 to 800 nm of three nickel nanoclusters respectively. The black lines represent experimental results, the red lines represent calculated ones. The arrows marked in (b), (d) and (f) are the calculated optical gaps of these nickel nanoclusters.

Table S1. The calculated HOMO-LUMO gaps of $Ni_n(SCH_3)_{2n}$ (n = 4, 5 and 6) by TD-DFT.

Nanoclusters	HOMO-LUMO Gap (eV)	λ (cm^{-1})
$Ni_4(SCH_3)_8$	3.17	391.3
$Ni_5(SCH_3)_{10}$	3.35	370.2
$Ni_6(SCH_3)_{12}$	3.45	359.7